Spectral response of Fabry–Pérot plasmonic optical resonators

MOSTAFA A. EL-AASSER[a,b,*], S. A. MAHMOUD[a,c]
[a]*Physics Department, Faculty of Science, Northern Border University, Arar, Saudi Arabia*
[b]*Physics Department, Faculty of Science, Ain Shams University, Cairo11566, Egypt*
[c]*Physics Department, Faculty of Science, Minia University, Minia, Egypt*

In this paper, Nano-Plasmonic Optical Resonator design of Fabry–Pérot type is proposed. It is an array of metal nanorods separated from a metal film by a dielectric layer. Some plasmonic optical resonators are briefly reviewed. Modeling and simulation of the spectral properties of the electric field in the resonator are presented. Tuning the resonance wavelengths at various resonator parameters of dimensions and materials is studied. The highest electric field enhancement is obtained for silver (~ 370). The field enhancement in Aluminum is almost one third that of Noble metals. Comparison of the field enhancement (between Al versus Be, Cr, Ni, Pd, Pt, Ti, and W) as non-plasmonic metals is investigated. Among all considered metals, Aluminum has the largest spectral width spans NIR, visible, and UV regimes. Nearly complete absorption is obtained at certain resonance wavelengths. The numerical calculations are carried out using the finite difference time domain (FDTD) method. The proposed design is simple to be manufactured and quite efficient for many applications in nanophotonics, surface sensing, and plasmonic solar cells.

(Received April 6, 2017; accepted August 9, 2017)

Keywords: Nanoresonators, Plasmonics, Optical nanoantenna, Field enhancement, Plasmonic sensors

1. Introduction

Metallic nanostructures have been of great importance in nanophotonic applications because of their capability of subwavelength confinement and enhancement of light, bringing their energy to nanoscale beyond the diffraction limit [1-6]. Nanoscale Plasmonic optical resonators open the road to so many applications like plasmonic nanosensors, near-field trapping techniques [7,8], high-resolution nanoimaging [9,10], high efficient photovoltaics [11], nanoscale photodetectors [1,12], efficient light coupling in quantum dots and single molecules [13-18].

Special interest has been shown in the resonant nanostructures that are quite like conventional Fabry-Perot resonators [19–27]. Metal-insulator-metal (MIM) or insulator-metal-insulator (IMI) configurations have been considered to achieve resonance by multiple reflections of slow SPP modes (gap and short-range surface plasmon modes, respectively) from the edges of the obtained structures. Plasmonic IMI structures revealed significant radiative losses more than MIM nanoresonators. This was attributed to large electric dipole moments associated with the fundamental resonance modes [18]. MIM resonators with gap surface plasmons (GSPs) have shown significant advantages as compared to IMI nanorod resonators therefore they have been a matter of research concern [28, 30]. Details of analysis of plasmonic optical resonators (PORs) could be found in [20, 31, 32]. Cavity quality factors up to ~20 were obtained for such resonators [33]. The optical properties were obtained analytically for subwavelength plasmonic MIM resonators and for their combination [34]. They applied the same formalism to a combination of two independent resonators. Several studies of PORs have so far been mainly confined to the structures where the same truncation was carried out for more than one layer in a MIM structure [20, 31–35]. It was shown that a finite-width metal rod close to a metal surface ensures efficient reflection of GSPs at rod edges, forming an efficient POR [22]. The fundamental properties and design of plasmon resonant nanostructures were also presented in [36-45]. A theoretical study of the optical properties of metallic nanorod antennas was formulated based on an interference Fabry-Perot model. The SR-SPP reflection amplitude and phase pickup upon reflection were calculated using the finite difference frequency domain (FDFD) method [46]. The scattering cross section and field enhancements in IMI resonators were analyzed using a surface integral equation method in [21, 24]. SPP and Gap Plasmon resonators have been studied and analyzed using the Green's function surface integral equation method. They showed the transition from a SPP resonator to a gap plasmon polariton resonator by varying the gap size [32]. Plasmonic color printing with subwavelength resolution was demonstrated using FPORs [47]. The optical response of PORs was described by a generalized cavity model which takes into consideration the nonlocal response of the metals arising from interactions between free electrons inside the jellium [48]. Polarization conversion and polarization controlling was presented using an array of PORs [49, 50]. A semi-analytical theoretical treatment of the spontaneous optical emission and coupling between dipole emitters and dissipative nanoresonators was used to calculate the electromagnetic response of systems that are governed by a small number of resonance modes [51]. Extreme near-field enhancement, for surface enhanced Raman scattering

and sensing applications, was demonstrated by the help of Fabry-Perot type nanogap resonators. The resonance is defined by the gap width and vertical elongation instead of the rod geometry [52]. An efficient launching of unidirectional SPPs with focused Bessel and Airy profiles have been experimentally realized by the help of aperiodic PORs [53, 54]. A multilayered gap surface plasmon resonator were numerically investigated as an efficient broadband visible light absorber with average simulated absorption of 93% [55].

In this work, the modeling and simulation of the spectral properties of electric field (Intensity) enhancement in Fabry-Perot PORs (FPORs) are demonstrated. The field enhancement due to resonant plasmonic excitations and tuning the resonance wavelength are presented. The effect of device dimensions and materials on the field enhancement is presented. The calculations are carried out using FDTD method.

2. Modeling and simulation

FPOR, shown in Fig. 1(a), is a subwavelength metal grating on a metal film separated by a dielectric spacer in one dimension. h, td, and t, denote to the metal rods height, dielectric layer and bottom metal thicknesses, respectively. The rod diameter and the unit cell periodicity are d and p, respectively. The physical principles for the considered resonator structures are like those of a conventional Fabry-Perot resonator. The GSPs guided by the dielectric between the metal rod and the bottom metal film experiences multiple reflections from the terminations (edges) of the rods. The radiation losses at the edges of the rods are due to electric dipole radiation caused by the oscillating opposite charges across the dielectric. However, because the size of this electric dipole moment is ~t_d (i.e., in tens of nanometers which are much smaller than the wavelength), these radiation losses are significantly weaker than those in the case of the IMI resonators [37]. In this work, a plane wave is incident normally on the surface of the FPOR. Strong electromagnetic coupling could occur between the surface metallic pattern and the metal film at selected wavelengths as recently suggested [37-40]. Since FPORs are basically two metal-dielectric interfaces separated by dielectric, the coupling between SPPs of the two interfaces gives rise to SPP super-modes exhibiting very interesting properties [57]. The calculations are carried out by MEEP simulation package, developed at MIT, which uses FDTD method under periodic boundary conditions. FDTD is one of the easiest, fastest, and most reliable electromagnetic eigenmode solvers of Maxwell's equations in different structures. The field enhancement spectra of the proposed FPOR are computed with the aid of MEEP at different dimensions and materials. Fine meshing of 5 nm is used in computations to maintain a high order of accuracy; such that 5 nm is equal to 1/80 of the shortest wavelength considered. The dielectric functions are obtained from [57], and the experimental data from [58]. Skin depth for gold in the wavelength interval (400-1600 nm) is estimated as (~2.8-5.5 nm). Since the metal film thickness (t = 200 nm) is substantially greater than the skin depth, the transmission of FPOR is almost null, therefore R + A = 1, where R and A are the reflection and absorption intensities, respectively.

FPOR can be modeled as LC resonance circuit as shown in Fig. 1(a). The inductance per unit length (L_m) of two parallel plates separated by a distance td can be given by $L_m = 0.5\mu_0\, t_d\, d$. $L_g = d/(\gamma\, \varepsilon_0\, h\, \omega^2_p)$, is the gap contribution to inductance per unit length, where γ is a factor considering the effective cross-sectional area of the metal rod. $C_m = 0.222\, \varepsilon_d\, \varepsilon_0\, d/td$ is the capacitance per unit length. $C_g = \pi\, \varepsilon_0/\ln(p - d)/h$ per unit length accounts for the contribution of the air gap between metal rods. Where μ_0, ε_0 and ε_d are the vacuum permeability, vacuum permittivity and dielectric function of the dielectric layer. Plasma frequency ω_p = 9.2, 8.9, and 8.7 eV for Ag, Au, and Cu, respectively. Accordingly, the resonance frequency for the LC circuit is given by [59-61] $\omega_r = \sqrt{\dfrac{C_g + C_m - \sqrt{C_g^2 + C_m^2}}{C_g C_m (L_g + L_m)}}$. Hence, the resonance wavelength is given by

$$\lambda_r = 2\pi c \sqrt{\frac{C_g C_m (L_g + L_m)}{C_g + C_m - \sqrt{C_g^2 + C_m^2}}}$$

The resonance wavelengths are plotted versus FPOR parameters h, t_d, d, p, and n in Fig. 1 (b-f). As the rod heights, h increases, a blue shift is occurred in the resonance wavelength as shown in Fig. 1(b). This is attributed to that the higher energy photons are the only photons that can penetrate through metal and reach the dielectric while the low energy photons are absorbed before reaching the metal-insulator interface. The same behavior is obtained as the dielectric layer thickness, td, increases as shown in Fig. 1(c). While increasing the rods diameters, a resonance wavelength red shift is obtained as shown in Fig. 1(d). The resonance wavelength is independent of the periodicity of the device cell as depicted in Fig. 1(e). In Fig. 1(f) a red shift is obtained as the dielectric refractive index, n increases.

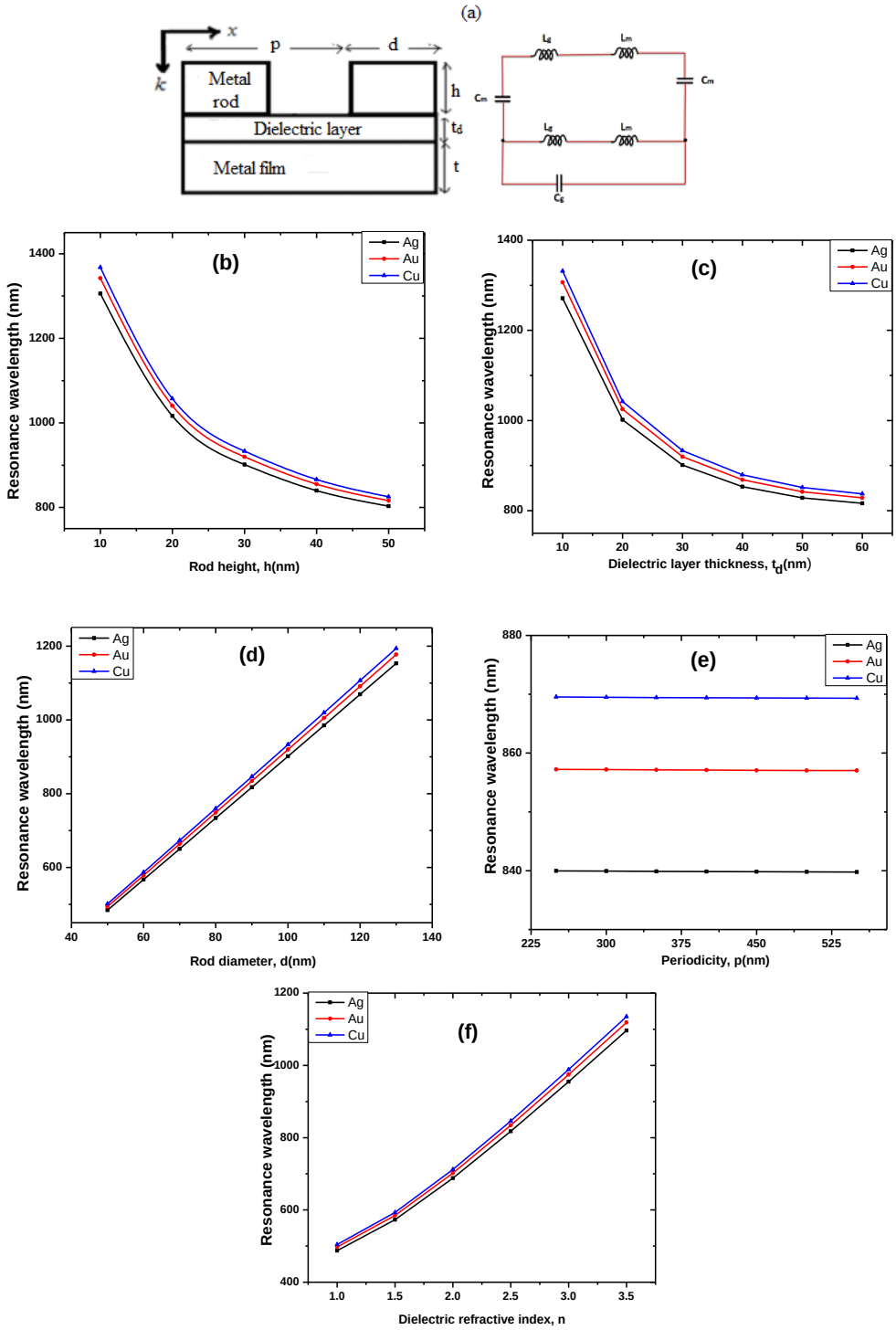

Fig. 1. (a) A scheme of FPOR with equivalent LC circuit, Resonance wavelength versus (b) Rod height, (c) Dielectric layer thickness, (d) Rod diameter, (e) Periodicity, and (f) Dielectric refractive index

3. Field enhancement under resonant excitation

PORs have shown that they are able to exhibit a significant field enhancement of an incident electromagnetic plane wave [36-39]. We report here the spectral investigation of the field enhancement under resonant excitation of the proposed FPOR. The electric field enhancement is computed (namely, the ratio $|E/E_0|^2 = I/I_0$). E_0 is the electric field amplitude of the incident plane wave, while E is the electric field at the maximum of the standing wave pattern of the field inside the resonator.

3.1. Resonator dimensions tuning

Gold is first selected for top rods and bottom metal film to investigate the effect of resonator dimensions on the field enhancement. The thickness of the bottom metal film (t) is chosen to be 200 nm to make sure that the device transmission is suppressed. The dimension's effect on electric field enhancement is studied as follows. The field enhancement spectrum is simulated at rod heights (h = 10-50 nm) while the other parameters are (periodicity, p = 400 nm, dielectric refractive index, n = 2.5, dielectric thickness, t_d = 30 nm, and rod diameter, d = 100 nm) as shown in Fig. 2. Increasing the rod height, h results in larger propagation losses and slower propagation speed, thus an increase in the effective mode index. Since the effective index is strongly wavelength dependent and inversely proportional to wavelength, a blue shift of resonance wavelength is obtained. This agrees with the prediction of the LC model as shown in Fig. 1(b). The blue shift value decreases approaching almost zero because the effective index saturates reaching a constant value at long wavelengths. Fig. 2(a) shows that the resonance wavelengths for electric field are 1321, 1241 nm at h = 10, 20 nm and 1205 for h = 30, 40, 50 nm. The blue shift is 80 nm from h = 10 to 20 nm but it is equal to 36 nm from h = 20 to 30 nm. No change in the peak wavelength is obtained when h = 30-50 nm. The highest electric field enhancement is obtained at h = 30 nm.

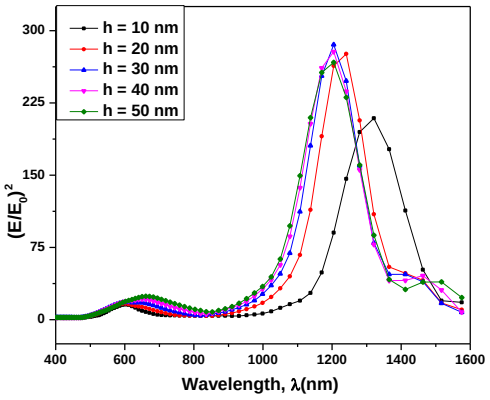

Fig. 2. Effect of rod height, (h) on the enhancement of the electric field, p = 400 nm, n = 2.5, t_d = 30 nm, and d = 100 nm

In Fig. 3 the field spectrum is calculated for dielectric thickness (t_d =10-60 nm) such that p = 400 nm, n = 2.5, h = 30 nm, d = 100 nm. The resonance wavelengths are inversely proportional to t_d, as predicted in Fig. 1(c). The obtained electric field resonance wavelengths are 1517, 1280, 1205 nm for t_d = 10, 20, 30 nm, respectively and 1170 nm for t_d = 40, 50, 60 nm as shown in Fig. 3. Therefore, the blue shift is 237, 75, and 35 nm for t_d = 10 to 20, 20 to 30, and 30 to 40 nm, respectively. The highest electric field enhancement is obtained at t_d = 30 nm.

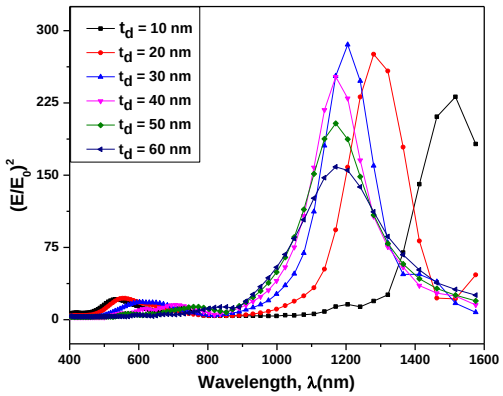

Fig. 3. Effect of dielectric thickness, t_d on the enhancement of the electric field, p = 400 nm, n = 2.5, h = 30 nm, d = 100 nm

For metal rod width (d = 50-130 nm) the field is calculated while p = 400 nm, n = 2.5, h = 30 nm, t_d = 30 nm as shown in Fig. 4. It shows that the obtained electric field resonance wavelengths are 853, 975, 1138, 1205, 1280, and 1412 for d = 50, 70, 90, 100, 110, and 130 nm, respectively. The resonance wavelength increases with increasing the rod width from d = 50 to 130 nm as predicted in Fig. 1 (d). The highest electric field enhancement is shown at d = 70 nm. As the rod diameters (d) increase, with constant periodicity, they got closer to each other therefore the dipole-dipole interactions and hence a red shift occurs. The red shifted optical spectrum could be due to dipole–dipole interactions between the nanogold rods.

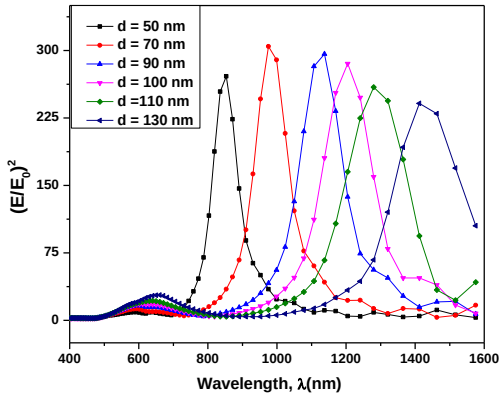

Fig. 4. Effect of widths of rod (d) on the enhancement of the electric field, p = 400 nm, n = 2.5, h = 30 nm, t_d = 30 nm

The effect of grating (unit cell) periodicity on the field enhancement (p = 250-550 nm) is shown in Fig. 5 while n = 2.5, h = 30 nm, t_d = 30 nm, d = 100 nm. Fig. 5 shows the electric field resonance at wavelength 1205 nm for p = 250

to 500 nm as predicted by the LC model as shown in Fig. 1 (e).

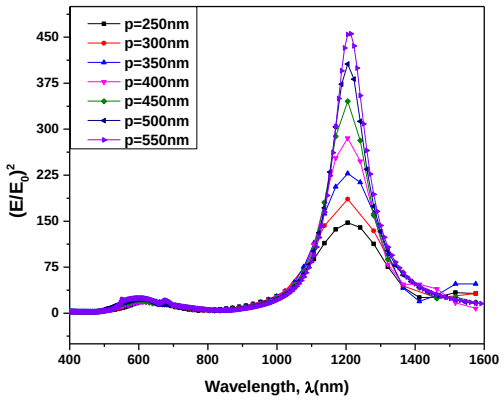

Fig. 5. Effect of grating period (p) on the enhancement of the electric field, n = 2.5,h = 30 nm, t_d = 30 nm, d = 100 nm

3.2. Resonator material tuning

The effect of the refractive index (n) for different dielectric materials on the electric field enhancement is studied. While the dielectric refractive index (n = 1-3.5), the field enhancement spectra is evaluated as shown in Fig. 6 such that p = 400 nm, h = 30 nm, t_d = 30 nm, d = 90 nm. The electric field resonance occurs at wavelengths 603, 759, 931, 1138, 1321, and 1519 nm for n = 1, 1.5, 2, 2.5, 3, and 3.5 respectively as shown in Fig. 6. A red shift is obtained as the dielectric index (n) increases as predicted in LC model shown in Fig. 1(f). The last two resonance wavelengths (1.3 and1.5 μm) are suitable windows in optical communications. The highest electric field enhancement is found at n = 2.

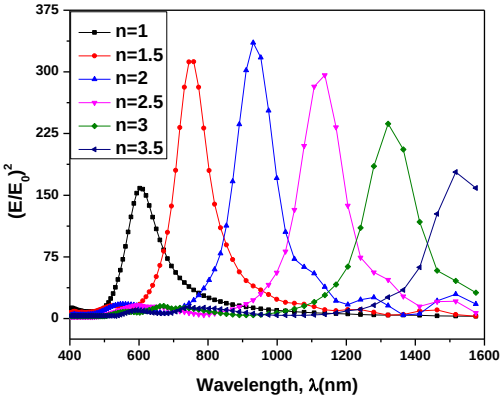

Fig. 6. Effect of refractive index (n) of the dielectric materials on the enhancement of Electric field, p = 400 nm, h = 30 nm, t_d = 30 nm, d = 90 nm

The optimized parameters (n = 2.5, h = 30 nm, t_d = 30 nm, d = 90 nm, p = 400 nm) are used to simulate the fields' spectra for Noble metals: Gold, Silver, and Copper as shown in Fig. 7. The electric field resonance occurs at wavelengths 1138, 1092, and 1078 nm for gold, silver, and copper, respectively, as in Fig. 7. The silver gives the highest electric field enhancement (~ 370) then copper then gold as shown in Fig. 7. This is attributed to the higher conductivity and electrons plasma density.

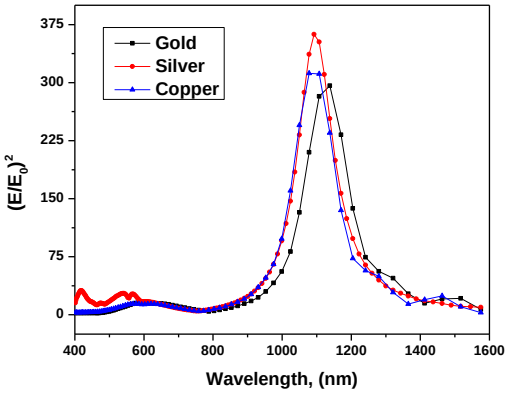

Fig. 7. Electric Field enhancement for Nobel metals, n = 2.5, h = 30 nm, t_d = 30 nm, d = 90 nm, p = 400 nm

The same parameters are also used to investigate the electric field enhancement spectra for the metals (Al, Be, Cr, Ni, Pd, Pt, Ti, and W) as shown in Fig. 8. The electric field enhancement in Aluminum (Al) is almost one third that for Noble metals (Au, Ag, Cu) by comparing Fig. 7 with Fig. 8. However, the electric field enhancement in Al is almost five times that in Be whose field enhancement is the highest among those for Cr, Ni, Pd, Pt, Ti, and W. Aluminum is distinguished from all other considered metals that it spans NIR, visible, and UV regimes. Therefore, it is a good choice for so many nanophotonic applications.

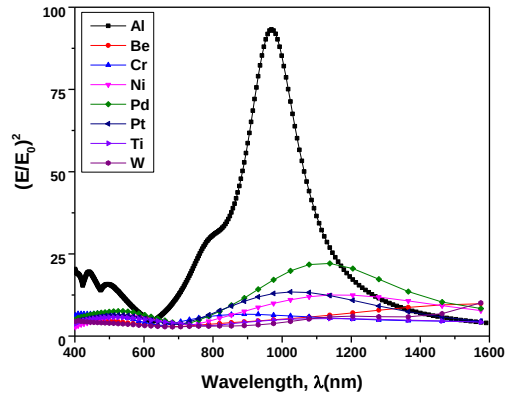

Fig. 8. Electric Field enhancement for different non-Noble metals, n = 2.5, h = 30 nm, td = 30 nm, d = 90 nm, p = 400 nm

4. Conclusions

FPOR is modeled, and its resonance excitations and electric field enhancement are studied. The effect of FPOR dimensions, dielectric material, and involved metals (Ag, Au, Cu, Al, Be, Cr, Ni, Pd, Pt, Ti, and W) on the field enhancement and resonance excitations is presented. Source of Gap surface plasmons (GSPs) with arbitrary phase is achieved. Its properties are strongly dependent on the dimensions of the gaps; the smaller the gap width, the larger the wavenumber. The developed physical interpretation can be used to account for previous observations [45, 62–64]. The localization of the enhanced field inside the thin dielectric layer opens excellent opportunities for using the considered FPOR arrays to enhance the efficiency of photovoltaic devices, gap plasmon sourses, and photodetectors design with better signal-to-noise ratio. The FPOR structures with high field enhancement can constitute a way for other efficient plasmonic applications such as surface-enhanced Raman spectroscopy and nano-optical sensors, single-molecule detection and identification.

Acknowledgements

The authors wish to acknowledge the approval and the support of this research study by the grant no. 05-06-1436-05 from the Deanship of Scientific Research in Northern Border University, Arar, KSA.

References

[1] J. A. Schuller, E. S. Barnard, W. Cai, Y. C. Jun, J. S. White, M. L. Brongersma, Nat. Mater. **9**(3), 193 (2010).
[2] W. L. Barnes, A. Dereux, T. W. Ebbesen, Nature **424**, 824 (2003).
[3] W. L. Barnes, J. Opt. A **8**(4), S87 (2006).
[4] M. Dragoman, D. Dragoman, "Nanoelectronics: Principles and Devices," Artech House, Boston, 2006.
[5] S. Lal, S. Link, N. J. Halas, Nat. Photonics **1**(1), 641(2007).
[6] A. Ashok, A. Arackal, George Jacob, Journal of Nanoscience and Nanotechnology **5**(4), 71 (2015).
[7] M. L. Juan, M. Righini, R. Quidant, Nat. Photonics **5**(6), 349 (2011).
[8] W. Zhang, L. Huang, C. Santschi, O. J. F. Martin, Nano Lett. **10**(3), 1006 (2010).
[9] J. N. Farahani, D. W. Pohl, H. J. Eisler, B. Hecht, Phys. Rev. Lett. **95**(1), 017402 (2005).
[10] A. Weber-Bargioni, A. Schwartzberg, M. Schmidt, B. Harteneck, D. F. Ogletree, P. J. Schuck, S. Cabrini, Nanotechnology **21**(6), 065306 (2010).
[11] H. A. Atwater, A. Polman, Nat. Mater. **9**(3), 205 (2010).
[12] L. Tang, S. Latif, A. K. Okyay, D. S. Ly-Gagnon, K. C. Saraswat, D. A. B. Miller, Nat. Photonics **2**(4), 226(2008).
[13] A. Kinkhabwala, Z. Yu, S. Fan, Y. Avlasevich, K. Mullen, W. E. Moerner, Nat. Photonics **3**(11), 654 (2009).
[14] D. K. Gramotnev, S. I. Bozhevolnyi, Nat. Photonics **4**(2), 83(2010).
[15] Peter Muehlschlegel, H-J Eisler, Olivier J. F. Martin, Last Dieter W. Pohl, Science **308**(5728), 1607 (2005).
[16] P. Bharadwaj, B. Deutsch, L. Novotny, Adv. Opt. Photon. **1**(3), 438 (2009).
[17] L. Novotny, N. Van Hulst, Nat. Photonics **5**(2), 83 (2011).
[18] H. Liu, L. Zhang, X. Lang, Y. Yamaguchi, H. Iwasaki, Y. Inouye, Q. Xue, M. Chen, Nat. Sci. Rep. **1**(1–5), (2011).
[19] T. Søndergaard, S. I. Bozhevolnyi, Phys. Rev. B **75**(7), 073402 (2007).
[20] S. I. Bozhevolnyi, T. Søndergaard, Opt. Express **15**(17) 10869 (2007).
[21] T. Søndergaard, S. I. Bozhevolnyi, Opt. Express **15**(7), 4198 (2007).
[22] T. Søndergaard, S. I. Bozhevolnyi, Phys. Stat. Solidi B, **245**(1), 9 (2008).
[23] J. Jung, T. Søndergaard, J. Beermann, A. Boltasseva, S. I. Bozhevolnyi, J. Opt. Soc. Am. B **26**(1), 121 (2009).
[24] J. Jung, T. Søndergaard, S. I. Bozhevolnyi, Phys. Rev. B **79**(3), 035401 (2009).
[25] T. Søndergaard, J. Beermann, A. Boltasseva, S. I. Bozhevolnyi, Phys. Rev. B **77**(11), 115420 (2008).
[26] Yoichi Kurokawa, Physical Review B, Condensed Matter **75**(3), 035411 (2007).
[27] Zhanghua Han, Sergey I. Bozhevolnyi, Opt. Express **19**(4), 3251 (2011).
[28] H. T. Miyazaki, Y. Kurokawa, Phys. Rev. Lett. **96**(9), 097401 (2006).
[29] P. Bouchon, F. Pardo, B. Portier, L. Ferlazzo, P. Ghenuche, G. Dagher, C. Dupuis, N. Bardou, R. Haidar, J. L. Pelouard, Appl. Phys. Lett. **98**(19), 191109 (2011).
[30] Thomas Søndergaard, Sergey I Bozhevolnyi, Jesper Jung, Alexandra E. Boltasseva, Proc. SPIE **7099**, 70991G (2008).
[31] T. Søndergaard, J. Jung, S. I. Bozhevolnyi, G. D. Valle, N. J. Phys. **10**(10), 105008 (2008).
[32] J. Jung, T. Søndergaard, Proc. SPIE **6988**, 69881N (2008).
[33] G. Lerosey, D. F. P. Pile, P. Matheu, G. Bartal, X. Zhang, Nano Lett. **9**(1), 327 (2009).
[34] Charlie Koechlin, Patrick Bouchon, Fabrice Pardo, Riad Haïdar, Opt. Express **21**(6), 7025 (2013).
[35] G. Lévêque, O. J. F. Martin, Opt. Lett. **31**(18), 2750 (2006).
[36] T. Søndergaard, S. I. Bozhevolnyi, Phys. Rev. B **75**(7), 073402 (2007).
[37] G. Della Valle, T. Søndergaard, S. I. Bozhevolnyi Opt. Express **16**(10), 6867 (2008).
[38] D. K Gramotnev, A. Pors, M. Willatzen, S. I. Bozhevolnyi, Physical Review B **85**(4), 045434 (2012).

[39] T. Søndergaard, S. I. Bozhevolnyi, Opt. Express **15**(7), 4198 (2007).
[40] A. Dmitriev, T. Pakizeh, Mikael Käll, D. S. Sutherland, **3**(2), 294 (2007).
[41] Sergey I. Bozhevolnyi, Thomas Søndergaard, Opt. Express **15**(17), 10869 (2007).
[42] M. G. Nielsen, D. K. Gramotnev, A. Pors, O. Albrektsen, Opt. Express **19**(20), 19310 (2011).
[43] M. G. Nielsen, A. Pors, O. Albrektsen, Opt. Express **20**(12), 13311 (2012).
[44] A. Pors, S. I. Bozhevolnyi, Opt. Express **21**(3), 2942 (2013).
[45] Masashi Miyata et al. Nano Lett. **15**(8), 5609 (2015).
[46] E. S. Barnard, J. S. White, A. Chandran, M. L. Brongersma, Opt. Express **16**(21), 16529 (2008).
[47] Alexander Sylvester Roberts, Anders Pors, Ole Albrektsen, Sergey I. Bozhevolnyi, Nano Letters **14**(2), (2014).
[48] Mathieu Dechaux, Paul-Henri Tichit, Cristian Ciracì, Antoine Moreau, "Generalized cavity model and nonlocal effects in nanoslit arrays," arXiv Jan (2015).
[49] Sergey I. Bozhevolnyi, IEE Proceedings, 978-1-4799-3682-3/14/Sep 2014.
[50] Zeyu Lei, Tian Yang, Conference: Frontiers in Optics, San Jose, California United States, FW5D.3 (2015).
[51] Christophe Sauvan, J. P. Hugonin, I. S. Maksymov, Philippe Lalanne, Physical Review Letters **110**(23), 237401 (2013).
[52] Thomas Siegfried, Yasin Ekinci, Olivier J. F. Martin, Hans Sigg, Nano Lett. **13**(11), 5449 (2013).
[53] Z. Lei, T. Yang, Conference: Frontiers in Optics, San Jose, California United States, FTh3F.7 (2015).
[54] Z. Lei, T. Yang, Applied Physics Letters **108**(16), 161105 (2016).
[55] Hyungduk Ko, Doo-Hyun Ko, Younghak Cho, Il Ki Han, Applied Physics A **116**(3), 857 (2014).
[56] E. N. Economou, Phys. Rev. **182**, 539 (1969).
[57] A. D. Rakic et al., Appl. Opt. **37**(22), 5271 (1998).
[58] P. B. Johnson, R. W. Christy, Phys. Rev. B **6**(12), 4370 (1972).
[59] J. Zhou et al., Phys. Rev. Lett. **95**, 223902 (2005).
[60] H. Wang, L. Wang, Opt. Express **21**(S6), A1078 (2013).
[61] L. P. Wang, Z. M. Zhang, Appl. Phys. Lett. **100**(6), 063902 (2012).
[62] R. Ameling, D. Dregely, H. Giessen, Opt. Lett. **36**(12), 2218 (2011).
[63] Y. Chu, M. G. Banaee, K. B. Crozier, ACS Nano **4**(5), 2804 (2010).
[64] Y. Chu, K. B. Crozier, Opt. Lett. **34**(3), 244 (2009).

*Corresponding author: elaasser@gmail.com